Title: Amorphous photonic crystals and structural colors in the phase separation glaze

Authors: Pei Shi, Fen Wang, Jianfeng Zhu, Haibo Yang, Yi Wang, Yuan Fang, Biao Zhang, Jiahuan Wang

PII: S0955-2219(17)30716-1
DOI: https://doi.org/10.1016/j.jeurceramsoc.2017.10.036
Reference: JECS 11523

To appear in: *Journal of the European Ceramic Society*

Received date: 16-8-2017
Revised date: 17-10-2017
Accepted date: 19-10-2017

Please cite this article as: Shi Pei, Wang Fen, Zhu Jianfeng, Yang Haibo, Wang Yi, Fang Yuan, Zhang Biao, Wang Jiahuan.Amorphous photonic crystals and structural colors in the phase separation glaze.*Journal of The European Ceramic Society* https://doi.org/10.1016/j.jeurceramsoc.2017.10.036

Amorphous photonic crystals and structural colors in the phase separation glaze

Pei Shi, Fen Wang*, Jianfeng Zhu, Haibo Yang, Yi Wang, Yuan Fang, Biao Zhang, Jiahuan Wang

School of Materials Science and Engineering, Shaanxi University of Science & Technology, Xi'an 710021, PR China

Abstract

In this paper, the phase-separated structures and the effective refractive index of the sky-blue glaze of Jun ware were investigated to determine the forming conditions of structural colors caused by amorphous photons crystals. It showed that with separation structures of short range order and average diameter of 106-260 nm, the structural color of amorphous photons could be formed in the glaze. In order to verify them and study the effect of colorant by the experimental method, the phase separation glazes were prepared with different contents of iron ore slag. The results indicated that the addition of colorant not only increased the effective refractive index of glazes, but also darkened the glaze color and suppressed incoherent scattering. Therefore, structural colors deepened with the increasing of colorant contents. Deciphering the ancient nanotechnology could thus potentially help researchers prepare colorful glazes by the green environmental protection method.

* Corresponding author: Tel.: +8602986131687; fax: +8602986168188.
Email addresses: wangf@sust.edu.cn (Fen Wang)

Keywords: Phase separation glaze; structural colors; amorphous photons crystals; effective refractive index

1. Introduction

Liquid immiscibility is widespread in silicate melts, being exhibited by a variety of binary and multi-component, natural and technological silicate glasses. The phenomenon has been extensively studied in material science because of its importance for the production of certain types of glasses and glass ceramics [1-2]. For ceramic glaze, it is an old as well as young topic.

In terms of existence, the phase separation glaze is old. The phase-separated structures were found from ancient celadon glazes of the Shang-Zhou period. Moreover, exact results showed that the phase separation glaze wares were produced in the Liang-Tang Huaian kiln before 1400 years [3]. A lot of investigations have demonstrated that the liquid immiscibility is a common phenomenon in Chinese ancient ceramic glazes, such as the Changsha kiln of Tang dynasty, the Jun and Ru kilns of Song dynasty and the Jian and Jizhou kilns of Song and Yuan dynasties, etc. The amazing yohen temmoku of Jian kiln, blue-green glaze of Jun kiln and sky-green glaze of Ru kiln are the typical phase separation glazes with mysterious blue and a variety of artistic appearances [4].

In terms of scientific research, it is also young. In the late 1970s and early 1980s, the phase separation glaze began to be revealed by the Chinese [5]. The phase separation is not only a structure feature of ancient famous porcelains, but also a direct

or indirect influence on the artistic appearance of wares. The surface patterns of the Jian wares such as Temmoku, Hare's Fur and Oil Spot are believed to originate from phase separation of glaze melts and crystallization of iron oxides separation. At high temperatures, the phase-separation droplets were formed and aggregated by the surface tension and weight, while the α-Fe_2O_3 crystals precipitated from droplets and formed the surface patterns [6]. Additionally, the opalescence blue of the Jun and Ru wares are known as the result of the phase separation at the glaze surface. When the average diameter of phase-separation droplets was 1-100 nm, the opalescence blue was formed and contributed to coloring of the glaze [7-8]. Nevertheless, inspired by amorphous photonic crystals in the biological world, Yin et al. proposed the short-range ordered phase-separated structure which was the reason of the structural color of amorphous photons in the glaze for the first time. It was the physical origin of opalescence blue in the Jun and Ru glazes [9-10]. However, there are few further scientific researches about the formation mechanism of structural color by amorphous photons crystals and their effect on the glaze color.

In this paper, the microstructure of the sky-blue Jun glaze of Song dynasty was studied, aiming at investigating the correlation between phase-separated structures and structural color caused by amorphous photons crystals. In addition, in order to verify them and study the effect of colorant by the experimental method, we attempted to prepare the phase separation glazes with different contents of iron ore slag in the R_2O-RO-Al_2O_3-SiO_2-P_2O_5 basis system. This work would throw some light on the better understanding of ancient nanotechnology and its application in today.

2. Experimental procedure

2.1 Materials

The base glaze compositions were made by 60 wt% feldspar, 20 wt% quartz sand, 15 wt% calcite, 2 wt% talc and 3 wt% commercial grade calcium phosphate ($Ca_3(PO_4)_2$). Meanwhile, 15-35 wt% iron ore slag were added as the colorant. Chemical compositions of the raw materials are given in Table 1.

Table 1 Chemical compositions of the raw materials (wt%).

Raw materials	SiO_2	Al_2O_3	Fe_2O_3	CaO	MgO	K_2O	Na_2O	TiO_2	P_2O_5	LOI
Feldspar	68.00	15.00	0.20	0.60	0.50	13.00	2.00	-	-	0.70
Quartz	98.30	1.41	0.22	-	-	-	-	-	-	0.07
Calcite	0.38	-	-	55.87	0.37	-	-	-	-	43.38
Talc	68.02	0.12	0.20	0.80	30.86	-	-	-	-	-
Iron ore slag	26.82	11.83	42.20	6.06	0.41	6.20	-	6.12	0.38	-

2.2 Glaze preparation

The raw glaze slurry was prepared by directly milling the starting materials which was weighted before with 70 wt% water, 0.5 wt% sodium carboxyl methyl cellulose (CMC), 0.2 wt% sodium tripolyphosphate (STPP) at a rate of 300 r/min for 40 min. The glaze slip was sieved and the density was adjusted to 1.5g/cm^3 by water. Then the glaze slip was applied to the biscuits test piece (Ø 4-5 cm) by dipping. After dried, the test pieces were fired at a heating rate of 3 °C/min to 900 °C and 1.5 °C/min to 1190

°C, and then insulated for 45 min at this temperature under an oxidizing atmosphere. Finally, the samples were cooled down to room temperature naturally in the furnace.

2.3 Characterization techniques

The sky-blue ware shard excavated from the Jun kiln site of Yuzhou Country, Henan Province was provided by the Palace Museum. The reflectance was obtained by using a UV/Vis/NIR spectrophotometers (Cary 5000, USA). And the phase composition of the test piece was identified by X-ray diffraction (XRD) using a D/max 2200PC X-ray diffractometer (Japan) with Cu K_α radiation (λ=1.5406 Å). Meanwhile, the samples were measured at a scanning rate of 8 °/min in the 2θ range of 10-50° under 40 kV and 100 mA. The microstructure of the samples was investigated by scanning electron microscopy (SEM) equipped with energy dispersive spectrometry (EDS). Before the testing, the surface of the samples was etched using 1 vol% HF for 20 s to expose the crystals and phase separation structures. Transmission electron microscopy (TEM) at 200 kV (Tecnai G2 F20, America) was used to study the microstructure of powder samples.

3 Results and discussion

Fig. 1 (a) shows the appearance of the Song dynasty sky-blue ware shard of Jun kiln. There were some pores and light-colored flow lines on the glaze surface. Moreover, its opacity was high like other Jun glazes. Since the physical appearance were greatly influenced by the crystallization behavior of glazes, it was necessary to clarify the formation of various crystalline phases created in the ancient sky-blue glaze. The XRD pattern of the Jun sky-blue glaze is shown in Fig. 1 (b). The characteristic

amorphous hump could be seen within the 2θ≈15-35° range in the sample, which was associated to a large amount of aluminosilicate glass. Meanwhile, some crystallization peaks, corresponding to silicon dioxide of two polymorphic forms (SiO_2, PDF#76-0932 and PDF#74-0814), were also detected in the sample. They were probably from the starting composition. The higher crystalline content could lead to the lower transparency. Consequently, the opacity of glaze surface was high.

Fig. 1. Appearance and XRD pattern of sky-blue glaze of Jun ware.

Fig. 2 displays the SEM images and EDS analysis of the etched Jun glaze surface. It could be clearly seen that some aggregate crystals disorderly distributed in the unetched glass phase (A), while the glass phase around it (B) had been etched by the HF (Fig. 2 (a)). The chemical composition of crystals was analyzed by EDS in Fig. 2 (b). It showed that the crystal was rich in Si and O. Combining with the XRD analysis in Fig. 1 (b), the main phase in dark area was quartz. It was because of the aggregate quartz that pores appeared on the glaze surface. The enlarged figures of A and B are shown in Fig. 2 (c) and (d). Apparently, the interconnected phase-separated structures were formed in the region A, and remained structurally intact after etching. On the contrary, the discrete droplet phase-separated structures were formed in the region B,

as well as they had been broken by the HF. These phenomena were ascribed to the difference of silicon content. The glass phase around quartz had higher Si content than that of other places, causing higher viscosity and corrosion resistance. In the system of high viscosity, the phase-separation droplets might merge and adhere so that combined into the interconnected phase-separated structure. Nevertheless, no matter what formed small-sized phase-separation droplets or interconnected phase-separated structure in the system with low viscosity, at last, they would shrink and grow large-sized phase-separation droplets [11]. Therefore, the phase separation structures were different at region A and region B.

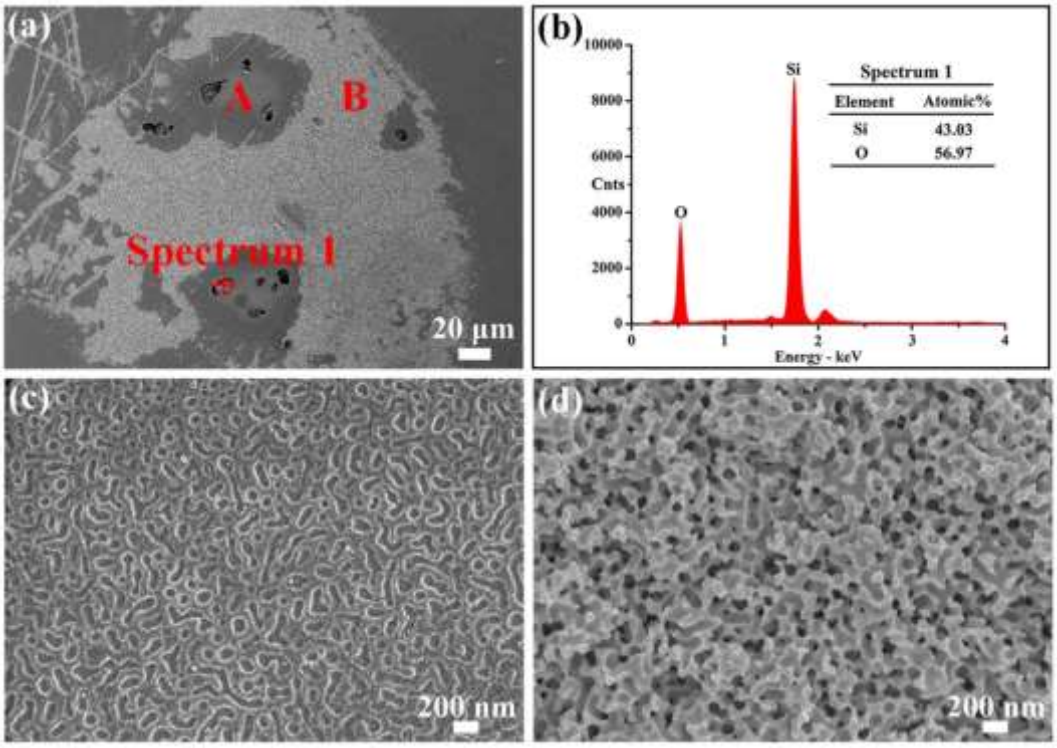

Fig. 2. (a) SEM image of the etched Jun glaze surface; (b) EDS spectra of the spectrum 1; (c)-(d) Enlarged images of A and B.

STEM-HAADF images in Fig. 3 reveal the unetched phase-separated structures of the sky-blue glaze. The interconnected and discrete droplet phase-separated structures (96 nm) were observed in the glass phase. Insets of Fig. 3 (a) and (b) show the corresponding 2D FFT images. The ring-shaped 2D FFT images clearly indicated that the phase-separated structures of the sky-blue glaze were in short range order rather than fully disordered.

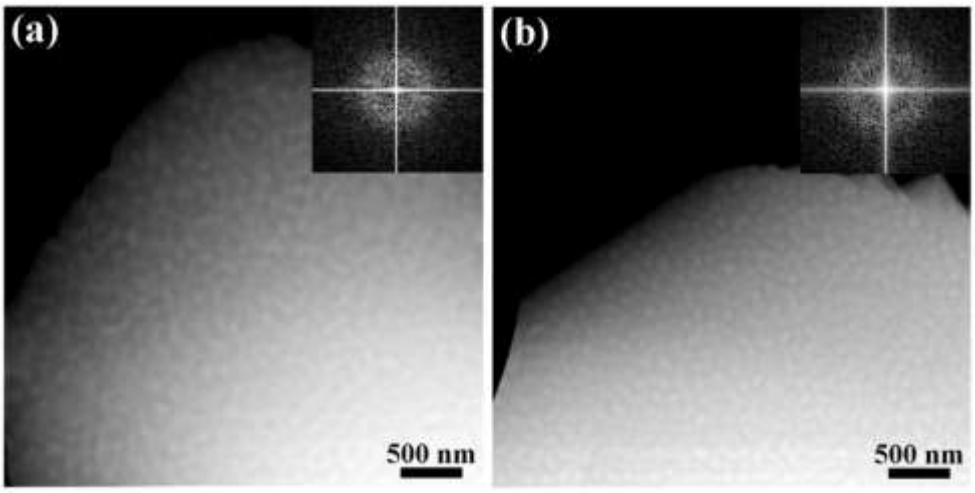

Fig. 3. STEM-HAADF images of the sky-blue glaze, (a) interconnected phase-separated structures; (b) discrete droplet phase-separated structures.

Jin et al. [12] investigated that the amorphous structures with only short-range order kept properties of the first band gap (pseudo-gap) of the crystalline structure. As electromagnetic waves whose frequencies were included within the pseudo-gap still struggled to propagate, the strongly reflected visible light by the pseudo-gap could be observed as the emission of a specific color by materials. It was referred to the structural color because the color was caused by the microstructures of materials rather than the

presence of pigments and dyes. Accordingly, pseudo-gap materials were being implemented as new ways to form structurally colored materials.

Yin et al. [9, 13] proposed that the colored glaze consisting of phase-separated structures showed the structural color. When the separation structures were complete disorder, the Rayleigh scattering ($d \leq 100$ nm) and Mie scattering ($d > 100$ nm) could be formed, which gave rise to the blue opalescence and milk white. Moreover, when the separation structures were in short-range order, the structural color by the amorphous photons crystals was formed on the glaze surface. On the basis of this argument, the sky-blue glaze of Jun ware might form the structural color of amorphous photons.

The STEM-HAADF images and EDS elemental analyses of the Jun glaze are shown in Fig. 4. As revealed in Fig. 4 (a) and (b), strong P, Ca, and Fe signals were detected in the microphase. The CaO of network modifier was no exception along with the P_2O_5 of network former to maintain electric neutrality. Meanwhile, the Fe_2O_3 as transitional metal oxides also played a role in network former. Most of them entered into the same phase with Ca and P.

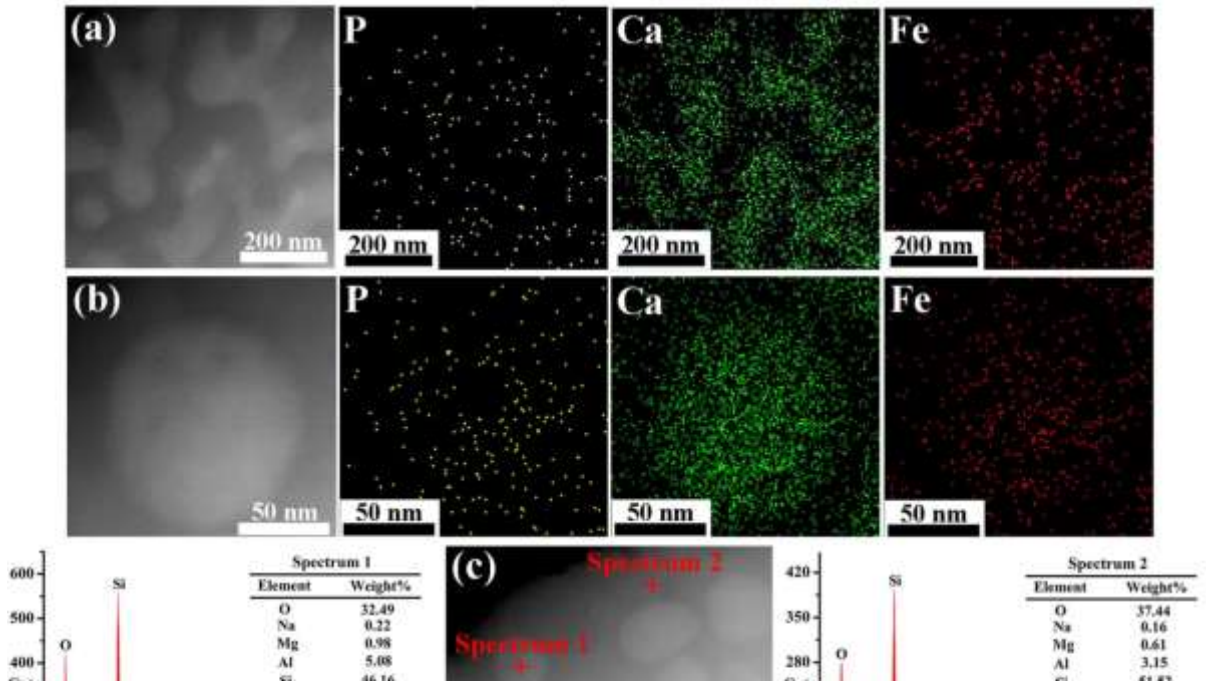

Fig. 4. STEM-HAADF/EDS elemental analysis of the sky-blue glaze, (a)-(b) STEM-HAADF images and elemental mapping images of P, Ca and Fe; (c) STEM-HAADF image and EDS spectrums of droplet phase-separated structure.

The refractive index of glass is calculated by using sum over states formula:

$$n = n_1 p_1 + n_2 p_2 + \ldots + n_i p_i \quad (1)$$

In this expression, p is the mole fraction of oxide in chemical compositions, and n is the refractive index calculation factor of oxide component. The STEM-HAADF image and EDS spectrums in Fig. 4 (c) revealed the compositional enrichment for the immiscible phases. According to the Eq. (1), the refraction index of the base phase (n_{Si}) was 1.522, while the refraction index of the microphase (n_P) was 1.569 with significant concentrations of P, Ca, and Fe. We applied the Maxwell-Garnett equation, to calculate the effective refractive index (n_e) of the sky-blue glaze, where φ was the volume fraction of microphase [14].

$$n_e = n_{Si}\left(\frac{2n_{Si}^{\ 2} + n_P^{\ 2} + 2\phi(n_P^{\ 2} - n_{Si}^{\ 2})}{2n_{Si}^{\ 2} + n_P^{\ 2} - \phi(n_P^{\ 2} - n_{Si}^{\ 2})}\right)^{1/2} \quad (2)$$

Based on the Eq. (2), the theoretical calculation of n_e was 1.564 with assuming φ = 90%. Since the forming mechanism of structural colors caused by amorphous photons crystals is also coherent scattering, an approximate expression for the scattering light wavelengths of the amorphous photons crystals is also given by the modified form of Bragg's law:

$$\lambda = 2d\sqrt{n_e^2 - \sin^2\theta} \quad (3)$$

In this expression, λ is the free-space wavelength of light, d is the interplanar spacing, and θ is the angle measured from the normal to the planes [15-18]. In the phase separation glaze, d is approximate to the average diameter of phase-separation droplets. Assuming that light is shining perpendicularly to the glaze surface, θ is 0 and $sin\theta$ is also 0. The Bragg's law could be expressed as [18]:

$$\lambda = 2dn_e \quad (4)$$

The theoretical calculation of λ was 300 nm with d = 96 nm and n_e = 1.564 by Eq. (4), which was not within the range of visible light wavelength (380-780 nm). Therefore, the structural color of the amorphous photons did not be formed in the sky-blue glaze of Jun ware. However, the gather and segregation of coloring elements increased their ions concentration in the phase-separated structures, which deepened the glaze color.

Due to the 1.5-1.8 refractive index in the glaze, the n_e is more than 1.5 and less than 1.8 by the Eq. (2). Assuming that the amorphous photons scatter visible light (380-

780 nm), the range of *d* should be from 106 nm to 260 nm according to Eq. (4). As a result, the formation condition of structural colors by amorphous photons crystals is that phase-separated structures need to be in short range order, while *d* is more than 106 nm and less than 260 nm. The phase-separation process is influenced by the variations of chemical compositions, viscosity of melts, and firing conditions such as temperature and atmosphere, and thereby these factors could be used to adjust the size of phase-separated structures and form structural colors [7].

Fig. 5 (a) presents the appearance and corresponding UV-Vis reflectance spectroscopy of the typical glazes with different iron ore residue contents. It was seen that the glaze appearance with 15 wt% iron ore residue exhibited brown with slightly blue, whereas the glaze with 35 wt% iron ore residue exhibited dark blue-green. Additionally, there was a weak reflectance peak at λ = 414 nm corresponded to the purple in the brown glaze. Nevertheless, two stronger reflectance peaks were observed in the spectrum of dark blue-green glaze, and the peaks at λ = 437 and 496 nm corresponded to the blue and green, respectively.

The XRD patterns of the samples with iron ore residue are displayed in Fig. 5 (b). In the samples, a diffuse hump could be observed, indicating its amorphous character. Moreover, there were some diffraction peaks attributable to quartz (SiO_2, PDF#86-2237) and omistenbergite ($CaAl_2Si_2O_8$, PDF#74-0814) in the glaze with 35 wt% iron ore residue. Among them, the quartz was probably from the starting composition, while the omistenbergite might be probably crystallized from the reaction of CaO, Al_2O_3 and

SiO_2. Due to a small amount of crystals, they did not have much of an impact on the glaze color.

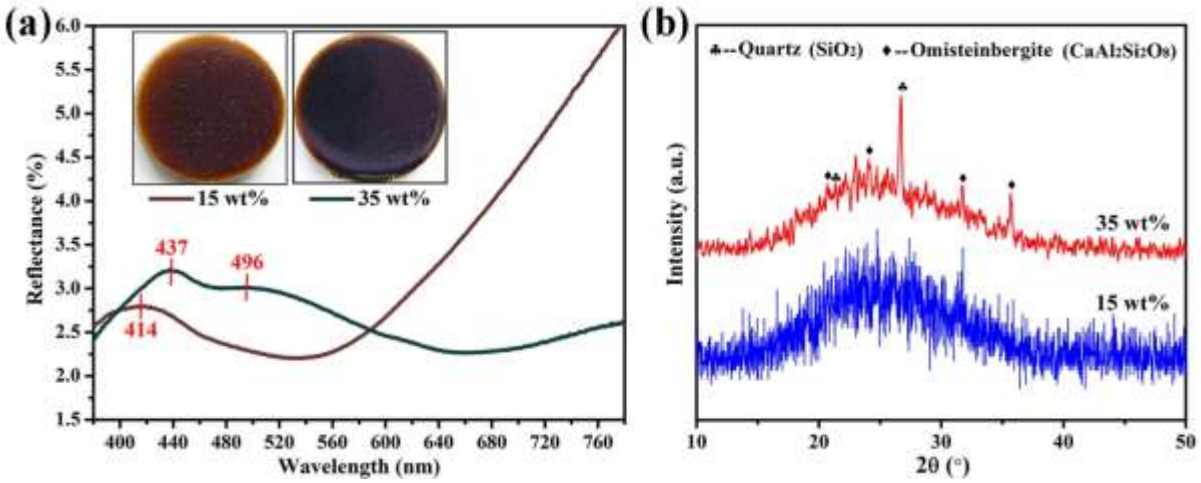

Fig. 5. (a) Appearance and UV-Vis reflectance spectroscopy; (b) XRD patterns of the glazes with different contents of iron ore residue.

The SEM images in Fig. 6 (a) and (b) revealed the microstructures of the etched glaze surfaces. It illustrated the discrete droplet liquid-liquid phase-separated structures appeared in the samples. Insets of SEM images presented the corresponding 2D FFT images. The ring-shaped 2D FFT images indicated that the phase-separation droplets belonged to the amorphous photons structures. The STEM-HAADF images and EDS spectrums of separation structures are shown in Fig. 6 (c) and (d). Based on the Eq. (1), (2) and (4), the theoretical calculations of λ were 412 nm (φ = 90%, d = 131 nm, n_e = 1.571) and 516 nm (φ = 90%, d = 149 nm, n_e = 1.733). Since d was obtained by statistical calculation, this was in reasonable agreement with experimental value of 414, 437 and 496 nm. The 414 nm was within the scope of purple wavelength (380-435 nm), and the 437 and 496 nm were within the scope of blue-green wavelength (435-560 nm).

Hence, the purple and blue-green appeared in the glaze surfaces with 15 and 35 wt% iron ore residue.

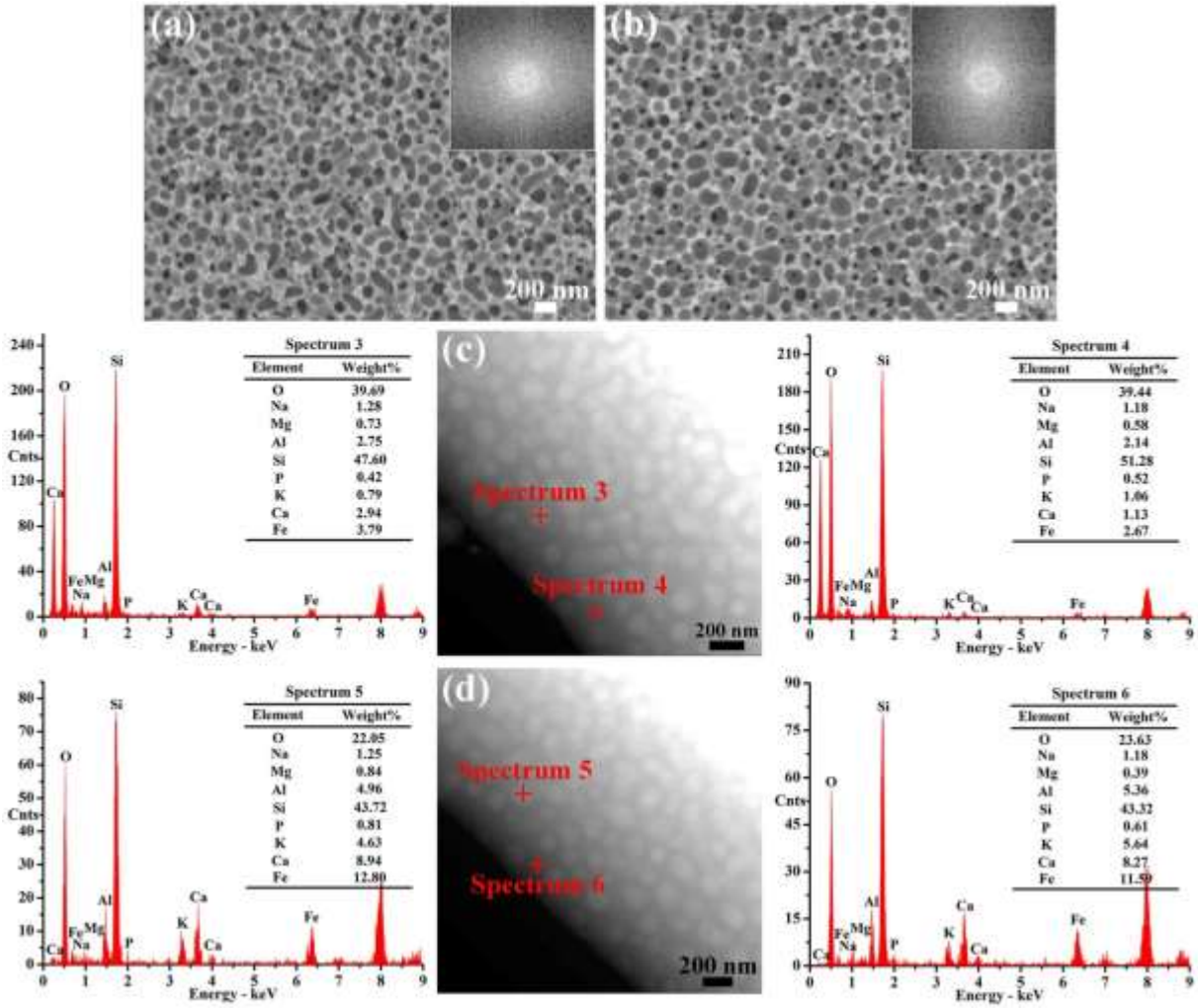

Fig. 6. SEM, STEM-HAADF images and corresponding EDS spectrums of iron ore residue glazes, (a) and (c) 15 wt%; (b) and (d) 35 wt%.

The addition of iron ore residue not only increased the effective refractive index (n_e) of glaze surfaces, but also deepened the glaze color. Cao et al. [14, 19-20] noticed

that the material of the amorphous array could produce recognizable structural colors independent of material thickness when a small amount of carbon black was added to the material. The reason for this was that wavelength-independent scattering (incoherent scattering) was suppressed by the added carbon black, and only wavelengths with the strongest scattering would escape the material before being absorbed. The more iron ore residue added, the deeper glaze color appeared, and more incoherent scattering suppressed (Fig. 7). Therefore, the stronger reflectance peaks were observed in the spectrum of dark blue-green glaze with 35 wt% iron ore residue.

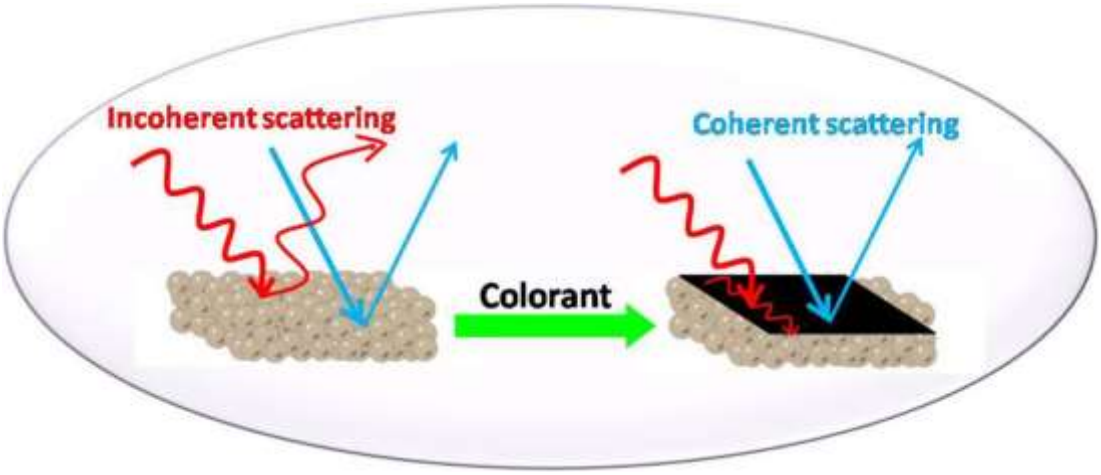

Fig. 7. Schematic optical properties of amorphous photons crystals with addition of colorant.

4 Conclusion

The Song dynasty sky-blue ware shard of Jun kiln was adopted as the test sample. The short-range ordered phase-separated structures were observed in the sky-blue glaze. Furthermore, most of coloring elements were distributed with Ca and P in the microphase. They increased the n_e of the glaze surface to 1.569. Based on the Bragg's

law, the theoretical calculation of λ was 300 nm. As a result, the structural color of amorphous photons did not be formed in the sky-blue glaze of Jun kiln. In addition, the separative-phase glazes were prepared with addition of 15-35 wt% iron ore slag. Since *d* of short-range ordered phase-separated structures was within the range of 106-260 nm, the structural color of amorphous photons appeared in the glaze surfaces. The more iron ore residue added, the deeper glaze color appeared and the more incoherent scattering suppressed. Therefore, the dark blue-green glaze with 35 wt% iron ore residue had stronger reflectance peaks of structural colors.

ACKNOWLEDGEMENTS

This work was supported by the National Foundation of Natural Science, China (51472153), the Shaanxi Science & Technology Co-ordination & Innovation Project, China (2015KTTSGY02-03, 2017TSCXL-GY-08-05) and the Graduate Innovation Fund of Shaanxi University of Science and Technology.

References

[1] G.M. Biggar, A re-assessment of phase equilibria involving two liquids in the system K_2O-Al_2O_3-FeO-SiO_2, Contrib. Mineral. Petr. 82 (1983) 274-283.

[2] M. Bogaerts, M.W. Schmidt, Experiments on silicate melt immiscibility in the system Fe_2SiO_4-$KAlSi_3O_8$-SiO_2-CaO-MgO-TiO_2-P_2O_5 and implications for natural magmas, Contrib. Mineral. Petr. 152 (2006) 257-274.

[3] X.Q. Chen, R.F. Huang, S.P. Chen, Phase-separation glazed porcelain in the 6th century A.D. - a study on Huaian ware of the Liang and the Tang dynasty, J. Chin. Ceram. Soc. 14 (1986) 147-152.

[4] H.W. Sun, X.Q. Chen, R.F. Huang, X.L. Zhou, L.M. Gao, Imitative process base of separative-phase glaze of Chinese dynasties, Ceramic (1994) 8-15.

[5] X.Q. Chen, R.F. Huang, S.P. Chen, D.F. Zhao, J.T. Wang, Liquid phase separation in iron oxide red glaze, Porcelain (1979) 1-24.

[6] C. Dejoie, P. Sciau, W.D. Li, L. Noé, A. Mehta, K. Chen, H.J. Luo, M. Kunz, N. Tamura, Z. Liu, Learning from the past: Rare ε-Fe_2O_3 in the ancient black-glazed Jian (Tenmoku) wares, Sci. Rep. 4 (2014) 4941.

[7] W.D. Li, J.Z. Li, Z.Q. Deng, J. Wu, J.K. Guo, Study on Ru ware glaze of the Northern Song dynasty: One of the earliest crystalline-phase separated glazes in ancient China, Ceram. Int. 31 (2005) 487-494.

[8] F. Wang, H.J. Luo, Q. Li, W.D. Li, Characteristic and coloring mechanism of the separative-phase colored ceramic, J. Chin. Ceram. Soc. 37 (2009) 181-186.

[9] H.W. Yin, Study on the coloring mechanism and preparation method of structural color, Fudan University 2008.

[10] L. Shi, Y.F. Zhang, B.Q. Dong, T.R. Zhan, X.H. Liu, J. Zi, Amorphous photonic crystals with only short-range order, Adv. Mater. 25 (2013) 5314-5320.

[11] C.G. Lin, C. Bocker, C. Rüssel, Nanocrystallization in oxyfluoride glasses controlled by amorphous phase separation, Nano Lett. 15 (2015) 6764-6769.

[12] C.J. Jin, X.D. Meng, B.Y. Cheng, Z.L. Li, D.Z. Zhang, Photonic gap in amorphous photonic materials, Phys. Rev. B 63 (2001) 587-588.

[13] P. Shi, F. Wang, J.F. Zhu, B. Zhang, T. Zhao, Y. Wang, Y. Qin, Study on the Five dynasty sky-green glaze from Yaozhou kiln and its coloring mechanism, Ceram. Int. 43 (2017**)** 2943-2949.

[14] J.D. Forster, H. Noh, S.F. Liew, V. Saranathan, C.F. Schreck, L. Yang, J.G. Park, R.O. Prum, S.J. Mochrie, C.S. O'Hern, H. Cao, E.R. Dufresne, Biomimetic isotropic nanostructures for structural coloration, Adv. Mater. 22 (2010) 2939-2944.

[15] B.Q. Dong , T.R. Zhan , X.H. Liu , L.P. Jiang , F. Liu , X.H. Hu , J. Zi , Optical response of a disordered bicontinuous macroporous structure in the longhorn beetle

Sphingnotus mirabilis, Phys. Rev. E. 84 (2011) 011915 .

[16] A.R. Parker, 515 million years of structural colour, J. Opt. A: Pure Appl. Opt. 2 (2000) R15-R28.

[17] A. Richel, N.P. Johnson, D.W. McComb, Observation of Bragg reflection in photonic crystals synthesized from air spheres in a titania matrix, Appl. Phys. Lett. 76 (2000) 1816-1818.

[18] S.G. Romanov, T. Maka, C.M. Sotomayor Torres, Diffraction of light from thin-film polymethylmethacrylate opaline photonic crystals, Phys. Rev. E. 63 (2001) 056603.

[19] Y. Takeoka, Angle-independent structural coloured amorphous arrays, J. Mater. Chem. 22 (2012) 23299-23309.

[20] Y. Takeoka, S. Yoshioka, A. Takano, S. Arai, K. Nueangnoraj, H. Nishihara, M. Teshima, Y. Ohtsuka, T. Seki, Production of colored pigments with amorphous arrays of black and white colloidal particles, Angew. Chem. Int. Edit. 52 (2013) 7261-7565.

Figure Caption

Figure Captions

Table 1 Chemical compositions of the raw materials (wt%).

Fig. 1 Appearance and XRD pattern of sky-blue glaze of Jun ware.

Fig. 2 (a) SEM image of the etched Jun glaze surface; (b) EDS spectrum of the spectrum 1; (c)-(d) Enlarged images of A and B.

Fig. 3 STEM-HAADF images of the sky-blue glaze, (a) interconnected phase-separated structures; (b) discrete droplet phase-separated structures.

Fig. 4 STEM-HAADF/EDS elemental analysis of the sky-blue glaze, (a)-(b) STEM-HAADF images and elemental mapping images of P, Ca and Fe; (c) STEM-HAADF image and EDS spectrums of droplet phase-separated structure.

Fig. 5 (a) Appearance and UV-Vis reflectance spectroscopy; (b) XRD patterns of the glazes with different contents of iron ore residue.

Fig. 6 SEM, STEM-HAADF images and corresponding EDS spectrums of iron ore residue glazes, (a) and (c) 15 wt%; (b) and (d) 35 wt%.

Fig. 7 Schematic optical properties of amorphous photons crystals with addition of colorant.

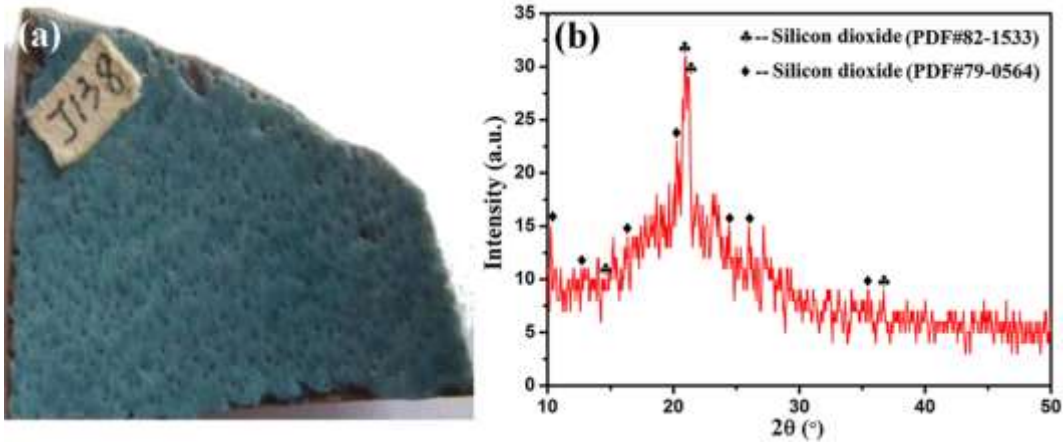

Fig. 1

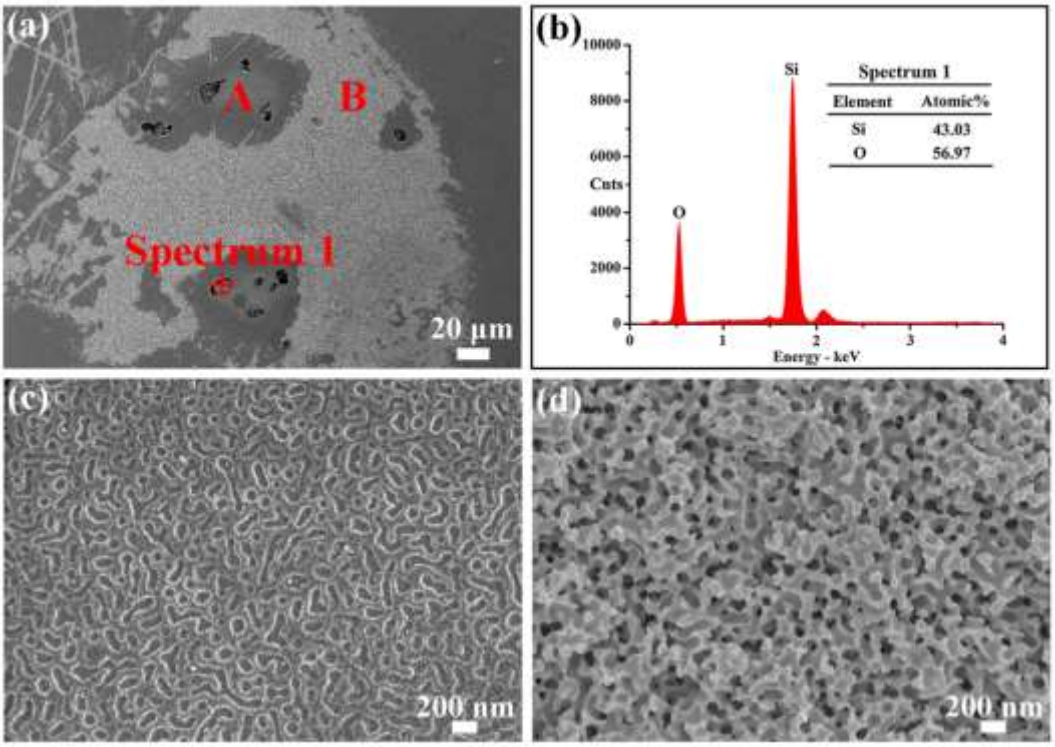

Fig. 2

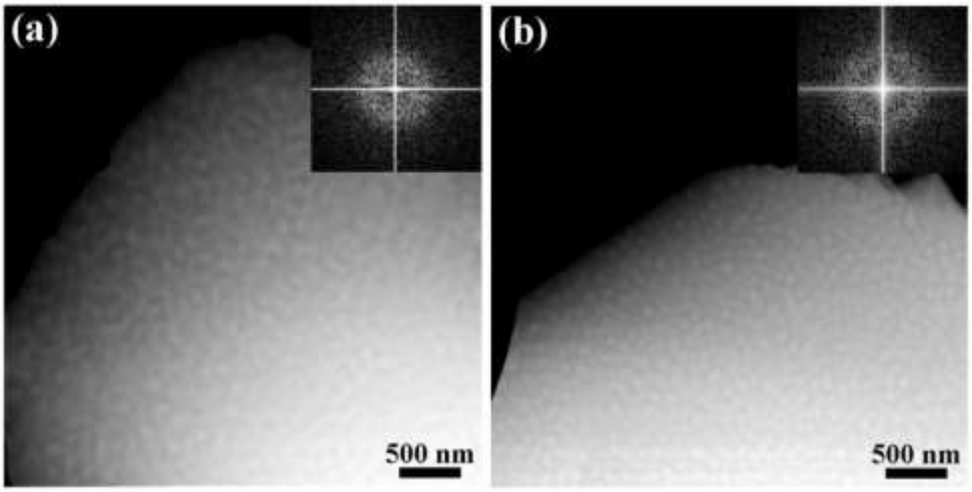

Fig. 3

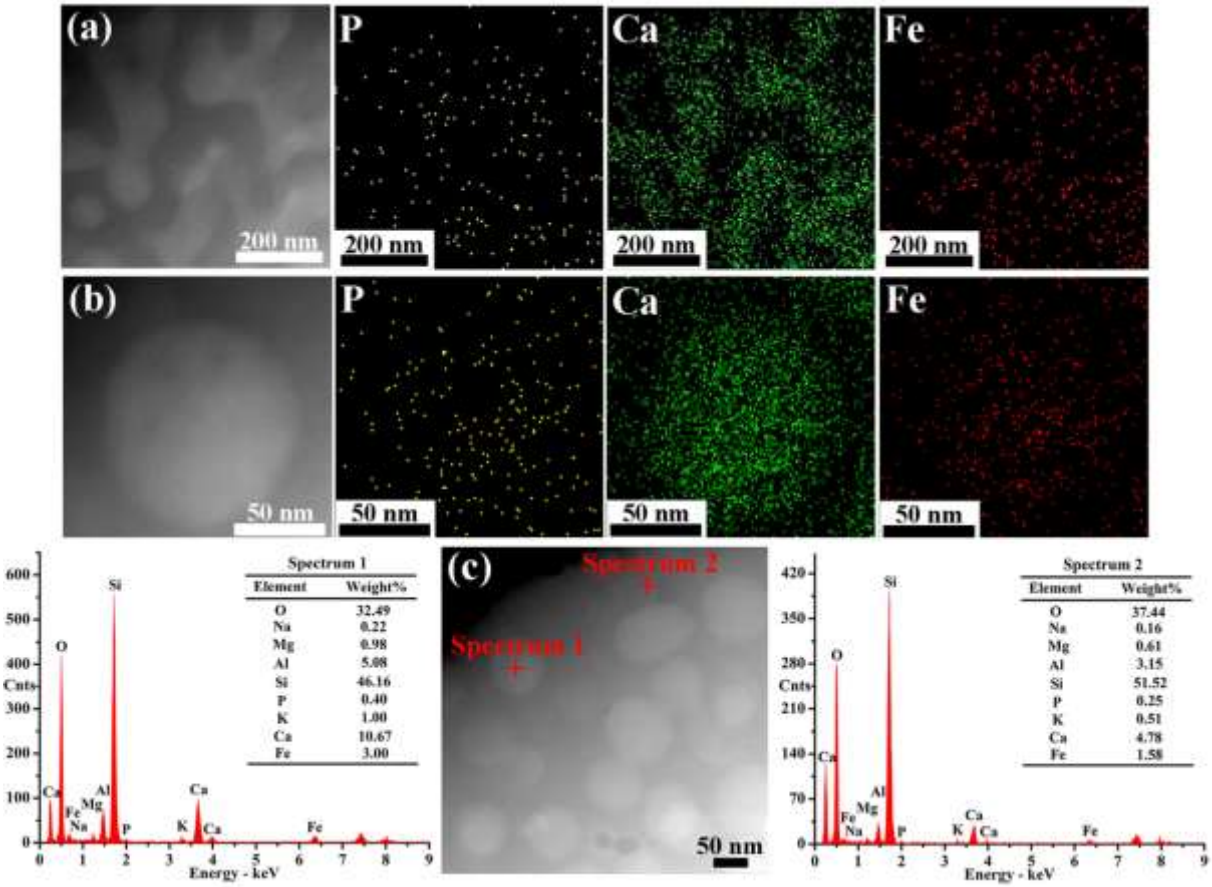

Fig. 4

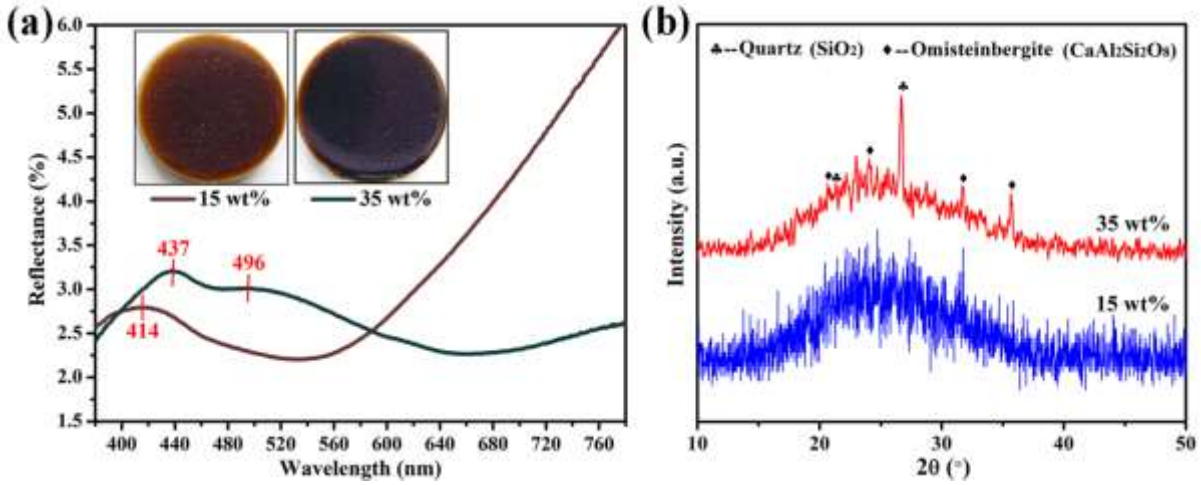

Fig. 5

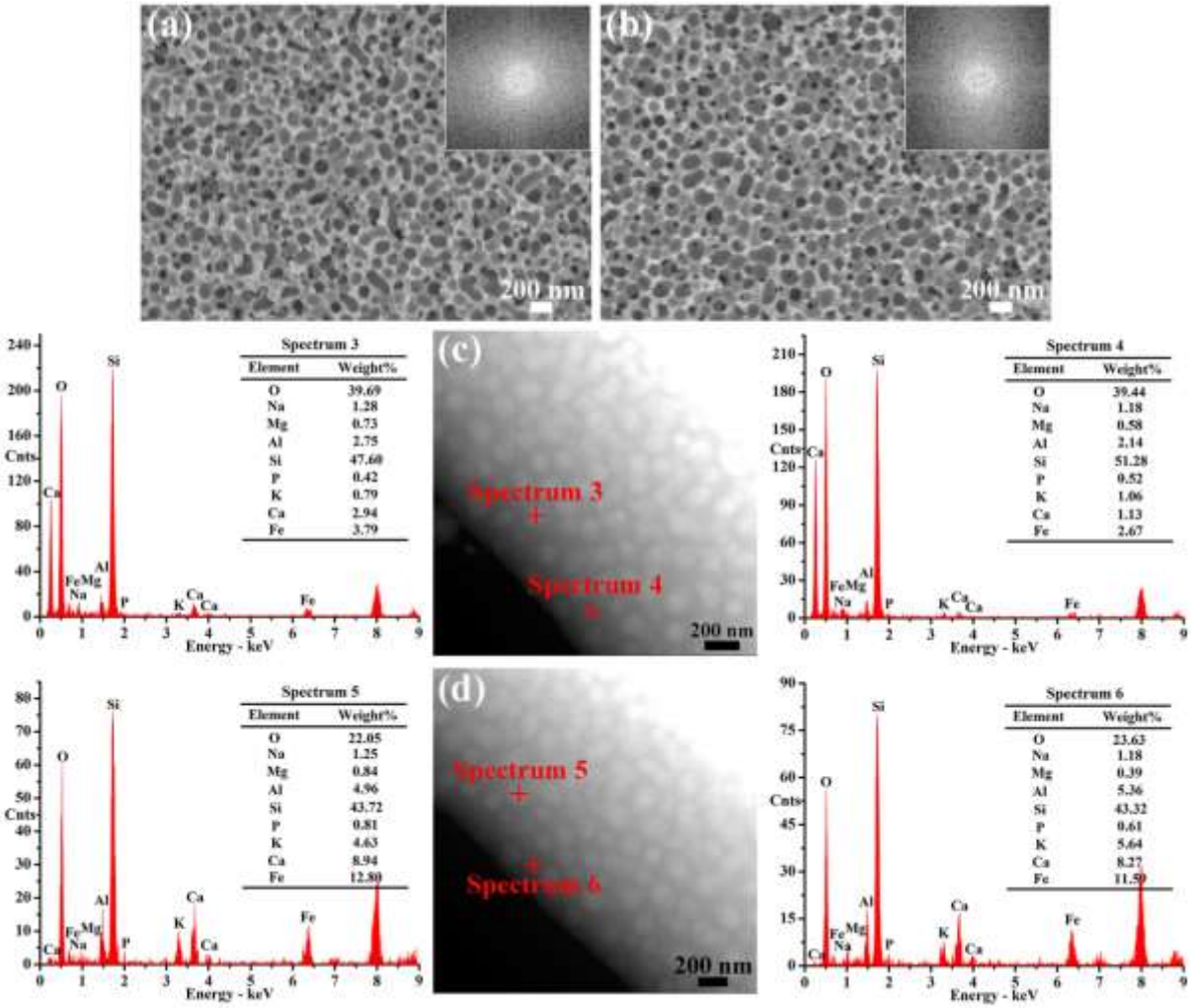

Fig. 6

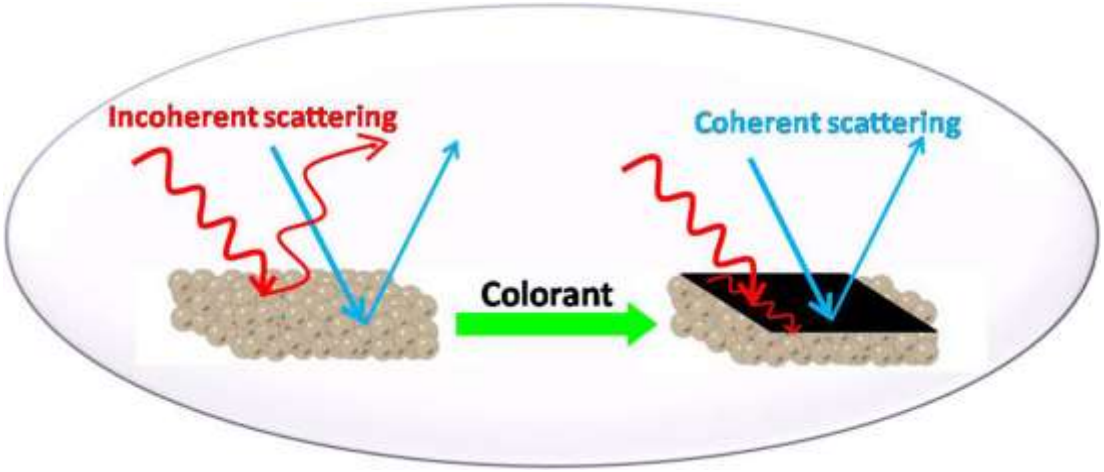

Fig. 7

Table 1

Raw materials	SiO_2	Al_2O_3	Fe_2O_3	CaO	MgO	K_2O	Na_2O	TiO_2	P_2O_5	LOI
Feldspar	68.00	15.00	0.20	0.60	0.50	13.00	2.00	-	-	0.70
Quartz	98.30	1.41	0.22	-	-	-	-	-	-	0.07
Calcite	0.38	-	-	55.87	0.37	-	-	-	-	43.38
Talc	68.02	0.12	0.20	0.80	30.86	-	-	-	-	-
Iron ore slag	26.82	11.83	42.20	6.06	0.41	6.20	-	6.12	0.38	-